Macroseismic intensity probability in the context of Bayesian Natural Neighbours

Franco Pettenati

fpettenati@ogs.it

Istituto Nazionale di Oceanografia e di Geofisica Sperimentale – OGS

Massimiliano Iurcev

Istituto Nazionale di Oceanografia e di Geofisica Sperimentale – OGS

Research Article

Keywords: macroseismic data, Voronoi tessellation, Natural Neighbour, Bayes theorem, soft prior, Lunigiana 1837 earthquake

Posted Date: June 17th, 2026

DOI: https://doi.org/10.21203/rs.3.rs-9713094/v1

Additional Declarations: No competing interests reported.

Macroseismic intensity probability in the context of Bayesian Natural Neighbours

Franco Pettenati and Massimiliano Iurcev

Istituto Nazionale di Oceanografia e di Geofisica Sperimentale – OGS, Trieste, Borgo Grotta Gigante, 42/c 34010 Sgonico, Trieste, Italy

Corresponding author: Franco Pettenati (fpettenati@ogs.it)

Abstract

The spatial distribution of seismic effects, quantified in terms of macroseismic intensity, forms the basis for a wide range of seismic analyses and hazard assessments. Voronoi tessellation provides an effective framework for representing discrete macroseismic observations in two dimensions. Building on this premise, we present a probabilistic method for assessing the reliability of intensity estimates at unobserved locations. The proposed approach reinterprets Sibson's Natural Neighbour weights within a Bayesian framework, treating them as prior probabilities over discrete intensity variables. The method is applied to site-specific hazard assessment in Campotosto (Central Italy) and to the Lunigiana earthquake of 11 April 1837 M_w 5.9, with comparisons to intensity prediction equations (IPEs). The results demonstrate that the method captures spatial variability consistent with macroseismic observations, providing a site-dependent measure of agreement between empirical data and model predictions. Furthermore, the probabilistic formulation enables estimating the spatial uncertainty inherent in Sibson interpolation. The Bayesian Natural Neighbours approach improves intensity mapping under data-scarce conditions and offers a flexible framework for probabilistic inference, consistency analysis, and integration with existing hazard models.

Key words: macroseismic data, Voronoi tessellation, Natural Neighbour, Bayes theorem, soft prior, Lunigiana 1837 earthquake.

1 Introduction

Voronoi tessellation (Okabe et al. 2000), is recognised as one of the best methods for representing qualitative variables (Burrough and McDonnell 1998). However, in the resulting map, all points within a polygon are implicitly the same intensity value as the generating site. Thus, any point inside a polygon in Fig. 1a), even if it differs from the observed data point (red dots), is represented by the same macroseismic intensity value. In this paper, we address the following question: how reliable is the value at a point inside a Voronoi polygon, other than the generating site itself? To answer this question, we reinterpret the deterministic Natural Neighbour (NN hereafter) interpolation scheme (Sibson, 1981) as a local probabilistic model for estimating discrete values. In our formulation, Sibson's method - traditionally geometric and deterministic - is recast as Bayesian Natural Neighbours (Bayesian NN hereafter), where interpolation weights are treated as probabilistic priors over discrete variables. Although this idea is not directly focused on interpolation, Sibson's method (1981) is potentially interesting both in general and for this new approach, for several reasons: i) it is based on Voronoi polygons; ii) it is parameter-free, which means it is objective and reproducible, since it relies solely on geometric and spatial criteria; iii) it is an exact interpolator, meaning it honours the empirical data at their site points; (iv), the obtained surface is derivable except in the data site; v) it is local, using only a minimal set of data.

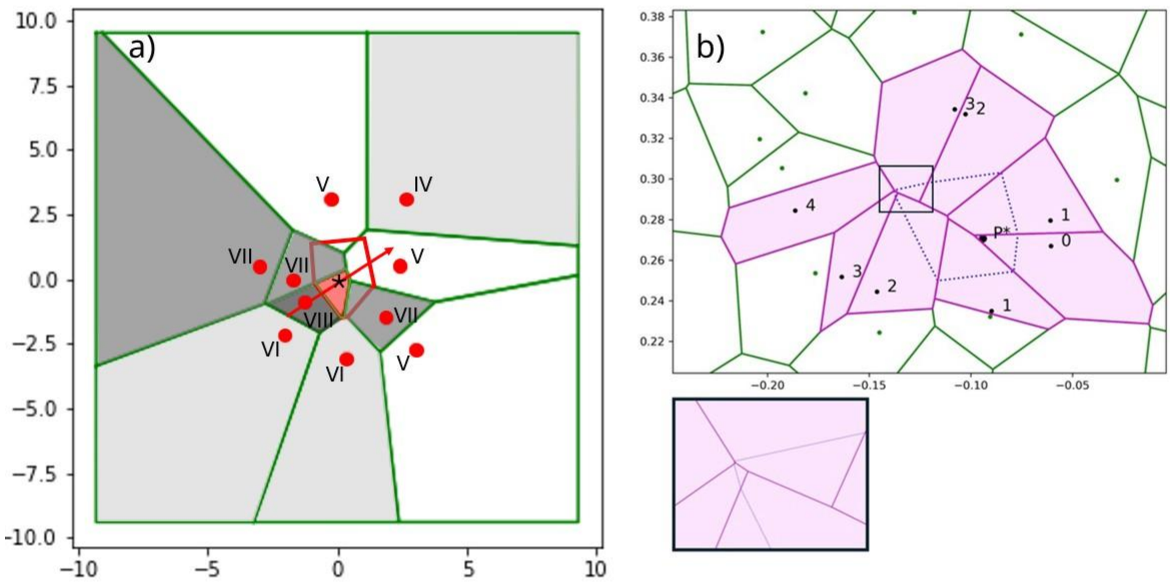

Fig. 1: a) Synthetic set of macroseismic data (red dots), tessellated with Voronoi polygons. The red polygon is the second-order Voronoi generated by the star point, inside the polygon of VIII. The red segment (indicated by the arrow) represents the path of the star point, illustrating the relative relationships between Sibson's weights in terms of probability in Fig. 2c; **b)** a Natural Neighbour

(NN) configuration ('*wreath'*) with the order of adjacent polygon '*wreath-order'* ω, till ω = 4 (see section 2). The small box at the bottom shows a detail of the configuration with the very small area of intersection with the adjacent polygon of ω-order = 4.

However, Sibson's method (1981) does not explicitly quantify interpolation uncertainty, which is fundamental in estimating physical quantities. In contrast, Kriging (Goovaerts 1997; Chilès and Delfiner 1999), by minimising the mean square error, naturally provides an associated uncertainty estimate. We attempted to compute the spatial uncertainty of the Natural Neighbours interpolation in a previous article (Iurcev and Pettenati 2023) using an approach based on the bidimensional extension of the Lagrange theorem (Mean Value Theorem).

We applied this Bayesian NN method to the macroseismic data to quantify the reliability of the data. In this work, the MDP (Macroseismic Data Points) are classified using quality scales MCS (Mercalli Cancani Sieberg - Mercalli 1902) as used in the CPTI15 Italian earthquake catalogue (Rovida et al. 2022). This catalogue includes approximately 5,000 events from the year 1000 to the latest update in 2022. The macroseismic data are important for various applications. The distributions of MDP are essential for estimating the location and magnitude of historical (pre-instrumental) earthquakes and for validating seismic hazard models. Designed to measure the 'strength' of earthquakes in the 19th century, during the pre-instrumental epoch, they were soon used to study the source of earthquakes by drawing the isoseismals (Mallet 1862; Kövesligethy 1907). Recent methods for characterising a pre-instrumental seismic source based on the distribution of MDPs, include that of Bakun and Wentworth (1997) for determining the epicentral location and magnitude; the QUake-MD model by Provost and Scotti (2020), which also provides a depth estimate; and the Boxer model by Gasperini et al. (1999), which allows estimating the fault direction. The KF Kinematic Function (Sirovich and Pettenati 2004, 2013; Gentile et al. 2004) also returns the fault plane solution. The KF is also used for calculating scenarios in MDPs (Sirovich and Pettenati 2009; Pettenati et al. 2011). Isoseismal mapping is still used today, although many researchers, especially in Italy, prefer to use coloured dots of MDP (Rovida et al. 2022) because of concerns about the objectivity of isoseismal tracing. Regarding objective methods, Pettenati et al. (1999), first applied a Voronoi tessellation to represent MDPs, while introducing objective and reproducible methods for plotting isoseismals was done by Sirovich et al. (2002), who correctly used the Sibson (1981) interpolation, and Worden et al. (2018), who used the Multivariate Normal Distribution, similar to the Objective Analysis (Barnes, 1964; Gandin, 1965) mainly applied in meteorology.

In the field of seismic risk, macroseismic studies use the curves of the Intensity Prediction Equation (IPE), as developed, for example, by Pasolini et al. (2008) and recently recalibrated by Lolli et al. (2024), to predict the Intensity Distribution Profile (MDP) at specific sites and to obtain information on earthquake magnitude. These methods provide a spatial representation of seismic events and play an important role in intensity-based risk assessments, particularly where historical earthquakes are the main source of available information. In this article, we present some examples demonstrating how the Bayesian NN approach can be applied in a risk-oriented context.

2 Methods

2.1 Preliminary considerations: the Voronoi tessellation and Sibson's method

The Voronoi tessellation (Okabe *et al.,* 2000, Aurenhammer et al. 2013) of a dataset of points with coordinates $\boldsymbol{x}_i$ in the two-dimensional Euclidean space $\mathbb{R}^2$, is defined as a set of convex polygons $\{V_i\}$ (Fig. 1a) that partition the plane Ω and satisfy the following property:

$$V_i \cap V_J = \emptyset;\ \forall i \neq j;\ \cup_i\, area(V_i) = \Omega \qquad (1a)$$

$$V_i = \left\{\boldsymbol{p} \in \mathbb{R}^2 \colon \forall j \neq i, d(\boldsymbol{p} - \boldsymbol{x}_i) < d\left(\boldsymbol{p} - \boldsymbol{x}_j\right)\right\} \quad (1b)$$

where *d* is the Euclidean distance between points.

To understand the Bayesian Natural Neighbours approach, first we introduce the set of polygons of the data points $\boldsymbol{x}_i$ as a '*wreath*' Ω (Fig. 1b). We define the '*wreath*' as the local neighbourhood domain $\Omega \subset \mathbb{R}^2$ around the control point $\boldsymbol{x}^*$. One polygon in the '*wreath*' contains $\boldsymbol{x}^*$, and it is defined as '*wreath-order'* as $\omega = 0$. The polygons adjacent to order-0 are defined as order-1, the polygons adjacent to a polygon of $\omega = 1$ are defined as order-2 and so on. Fig. 1b shows a control point $\boldsymbol{x}^*$ (red asterisk) that generates a '*wreath*' with a polygon till the $\omega = 4$ (see the small box in Fig. 1b). In the Supplementary S1 you can see a statistic of '*wreath-order*' estimated with a Montecarlo method.

The key question we now propose to answer is: how probable is a point $\boldsymbol{x}^*$ (test point) other than the generator site, to have the same intensity value? Before explaining the method, it is worth noting that, as the approach is based on the Voronoi tessellation of observation points, it is naturally suited to discrete and ordinal variables such as MDP. Let us consider a dataset of points with coordinates $\boldsymbol{x}_i$ in the two-dimensional Cartesian space $\Omega \in \mathbb{R}^2$, which generate a Voronoi tessellation V_i (of area A_i). The tessellation underpins Sibson's Natural Neighbours (NN) interpolation method [Sibson

1981], which identifies a unique set of natural neighbours for any interpolation point $\boldsymbol{x}^*$, namely the '*wreath*' (Fig. 1b). The point $\boldsymbol{x}^*$ generates a second-order new Voronoi cell V^* (shown in red in Fig. 1a) of area A^*. The intersection of areas A of V_i and V^* defines the Sibson interpolation weights:

$$w_i = \frac{(A_i \cap A^*)}{A^*} \qquad (2)$$

Recalling now the interpolation weights (3) for the value at $\boldsymbol{x}^*$, Sibson's method is a linear function

$$\boldsymbol{x}^* = \sum_i w_i f(x_i) \quad (3)$$

with the conditions

$$w_i \geq 0 \qquad (4a)$$

$$\sum_{i=1}^{n} w_i = 1 \text{ (normalization)} \qquad (4b)$$

2.2 Spatial interpretation of the Sibson scheme as a Bayesian approach

We refer to this reinterpretation as the Bayesian NN version of Sibson's method (1981). This interpolation technique is traditionally geometric and deterministic, based on the earlier article (Sibson 1980), where the coordinates of a point $\boldsymbol{x}^*$, given a spatial distribution of points $\boldsymbol{x}_i$ are uniquely determined. Here, we propose a probabilistic reinterpretation, in which the Sibson interpolation weights (Sibson 1980) are treated as prior probabilities over discrete variables.

Considering A_i $area(V_i)$ an uncountable infinite set under the conditions (1a): $A_i \cap A_j = \emptyset;\ \forall i \neq j$ (Fig. 1b), the Sibson's weights (2) can be formally interpreted as conditional probabilities:

$$w_i = P(A_i|A^*) = \frac{(A_i \cap A^*)}{A^*} \qquad (5)$$

This follows from the fact that the weights are positive (Eq. 4a), normalised, and represent relative area contributions. In other words, the Sibson weight w_i can be interpreted as the probability that a point belongs to polygon V_i, given that it lies within the area of the second-order cell V^*. Therefore, the overlap areas define not only a set of weights, but also a spatially informed probabilistic structure.

In terms of Bayes' theorem, the Sibson's weight w_i

$$P(A_i|A^*)A^* = P(A^*|A_i)A_i \quad (6a)$$

$$w_i A^* = P(A^*|A_i)A_i \qquad (6b)$$

Although Sibson weights can be formally interpreted within a Bayesian framework as conditional probabilities, in this study they are used as spatially informed prior probabilities for discrete MDP values. The proposed approach is therefore Bayesian-inspired (e.g. Friston et al., 2002) rather than fully Bayesian, as it does not introduce an explicit likelihood function. Instead, the spatial geometry implicitly defines a likelihood structure, while the weights are interpreted as spatial "soft priors". This last term follows the probabilistic concept of soft constraints discussed by Backus (1988). In the general version of Bayes' theorem, we have

$$w_i = \frac{P(A^*|A_i)A_i}{\sum_{j=1}^{n} P(A^*|A_j)A_j} \qquad (7)$$

here, A_i can be seen as the prior marginal probability, and $P(A^*|A_i)$ as the local dependence between values (the likelihood term): the probability of observing A^* given A_i, whilst the weights would act as posterior probabilities. Moreover, in the present formulation, the normalisation term plays a role analogous to the denominator of Bayes' theorem (see Eqs. 2 and 4), ensuring that the weights sum to unity. Indeed, $P(A^*|A_j) = \frac{(A^* \cap A_j)}{A_j}$ (Eq. 7) so simplifying the A_i at the top and bottom in the sum

$$\sum_{j=1}^{n} \frac{(A^* \cap A_j)}{A_j} A_j = \sum_{j=1}^{n} (A^* \cap A_j) = A^*$$

A^* is the priori probability that is the constant of normalisation (see equations 2 and 4).

Considering the set of MDP values I_i associated with the *wreath* defined around a target point $\boldsymbol{x}^*$, we define a prior probabilistic distribution for the intensity at $\boldsymbol{x}^*$ as:

$$P(I_i = k) = \sum_{i=1}^{12} w_i \cdot \delta_{k,round(I_i)} \qquad (8a)$$

where $\delta_{k,round(I_i)}$ is the Kronecker delta (equal to 1 if I_i=k, 0 otherwise)

$$\delta_{k,D_i} = \begin{cases} 1 \; if \; k = (I^*) \\ 0 \; otherwise \end{cases} \qquad (8b)$$

This soft prior directly represents the discrete probability distribution at $\boldsymbol{x}^*$ (e.g. in Fig. 1a), expressed as a weighted combination of observed intensities, where the weights are determined by the geometric contribution (shared Voronoi area) of each neighbouring point (see the Fig. 2a-b).

The reliability of the target point $\boldsymbol{x}^*$, located within the Voronoi polygon of *wreath-order* ω =0, can then be quantified as follows:

$$P_{rel} = P(I = I^*) = P\big(I^* = k_{inside(\omega=0)}\big) \quad (9)$$

Alternatively, the maximum reliability can be defined as the sum of the probabilities associated with all occurrences having the same intensity value assigned to the polygon of order ω =0:

$$P_{max} = P_{max}(I^* = k) = max\big(\textstyle\sum_{i=1}^{n} w_i \cdot \delta_{(I^*=k)}\big) \quad (10)$$

the exceedance probability is defined as:

$$P_{rel} = P(I > I^*) \quad (11)$$

Finally, the intensity at site s, can be estimated as the value corresponding to the maximum probability of the soft prior distribution (i.e. the maximum a posteriori estimate).

$$\hat{I}_s = argmax_k \, P(I_s = k) \qquad (12)$$

This is the Maximum a Posteriori (MAP) which preserves the discrete nature of macroseismic intensity and avoids the need for continuous interpolation between MDP classes.

3 Results

As the proposed approach is based on a data-driven interpolation scheme, it relies on the spatial distribution of observed data rather than an explicit physical model of the underlying phenomenon. The method is particularly suited to variables that are discrete and ordinal, such as macroseismic intensity. Within this framework, we aim to assess the applicability of the method in seismology through a series of tests, with particular emphasis on seismic risk assessment. First, we examine the behaviour of Sibson weights (2), varying their spatial configuration and statistical parametres to evaluate their robustness. Subsequently, we present a set of applications, focusing on the potential use of the method in seismic hazard analysis. Finally, we present an application to assess the uncertainty of the Sibson (1981) interpolation, extending previous work (Iurcev and Pettenati 2023).

3.1 Soft-prior probability distribution in a site

Since the local characteristic (criterion (v) in the Introduction) of natural neighbour (NN) is considered (Sibson 1980), we first apply the Bayesian NN method to some individual sites to show the prior distributions and the relationship between the weights. Equations (8a) and (8b) define the soft prior discrete probability distribution of intensity at point $\boldsymbol{x}^*$, where the probability of each intensity level is calculated as a weighted combination of the neighbouring observations $\boldsymbol{x}_i$, with weights derived from NN interpolation. Considering the *wreath* in Fig. 1a, Fig. 2a shows the distribution of probability at the point $\boldsymbol{x}^*$ with coordinates x=0.; y=0. This point lies within the polygon of value VIII, with a probability of having the same value $P(I_i = 8) = 0.31$. Moving the point $\boldsymbol{x}^*$ to the position (x=1.2; y=0.8) inside a polygon with value V, the probability is $P(I_i = 5) = 0.70$ (Fig. 2b). In other words, $\boldsymbol{x}^*$ is associated with a normalised probability distribution (weights w_i) for a class of MDPs. If we translate the control point from coordinates x=-1.8: y=-1.2 to x=1.5: y=-1.0 (red arrow in Fig. 1a), Fig. 2c shows the mutual trends between weights in terms of probability (or reliability as in figure). Instead, in Fig. 2d the linear trend of intensity in the translation is reported, following the Eq. (3) and the expected singularity at the point of VIII measurement as criterion (iv) suggests. Further details are provided in Supplementary S2.

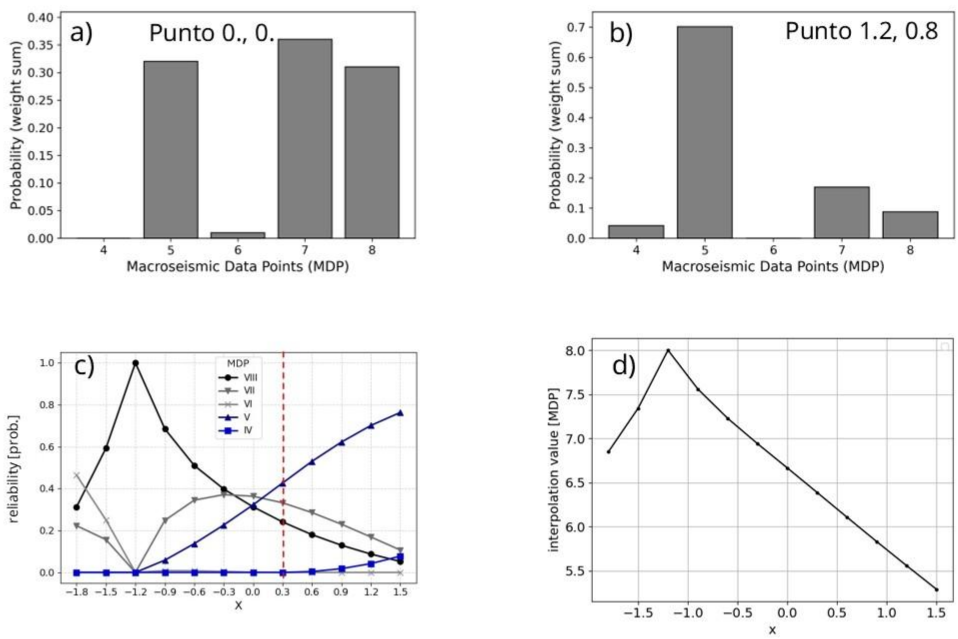

Fig. 2: a) The soft prior probability (or reliability) distribution, by Bayesian Natural Neighbour method (BNN) of star point in Fig. 1a (coordinates x=0.; y=0.) for the classes of MDP; **b)** the soft prior distribution of the point shifted to the position (x=1.2; y=0.8); **c)** the mutual trends between weights in terms of probability, translating the star point from coordinates x=-1.8: y=-1.2 to x=1.5: y=-1.0 (red arrow in Fig. 1a); the dotted red line marks the transition of the star point from polygon VIII to polygon V; **d)** linear trend of intensity in the translation from x=-1.8: y=-1.2 to x=1.5: y=-1.0, with the cusp discontinuity at the coordinates of point VIII (see criterion (iv) in the introduction).

We then examine an initial application to the seismic hazard of a single site. We select the site of Campotosto (Central Italy), an Italian municipality that is home to three dams (Moratto et al. 2023). It is an active seismic area, affected by many historical earthquakes. We selected the dataset of 27 earthquakes from the CPTI15 (Rovida et al. 2022) catalogue (Table 1), which contains at least 2 NN around the Campotosto site, which is deleted in the computation, according to the scheme

$$P_s^e(I = k) \qquad (13)$$

where *s* indicates the site; *e* the earthquake; k the MDP degree. In the case of MDP, with uncertainties between two contiguous MDP values (e.g. V-VI), we assigned a weight of 0.5 to each. Adding up the events and normalising for their number (n_e),

$$P_s(I = k) = \sum_e \frac{P_s^e(I=k)}{n_e} \qquad (14)$$

we obtain the cumulative and normalised prior distribution in Fig. 3. Table 2 summarises the values of probability for each intensity.

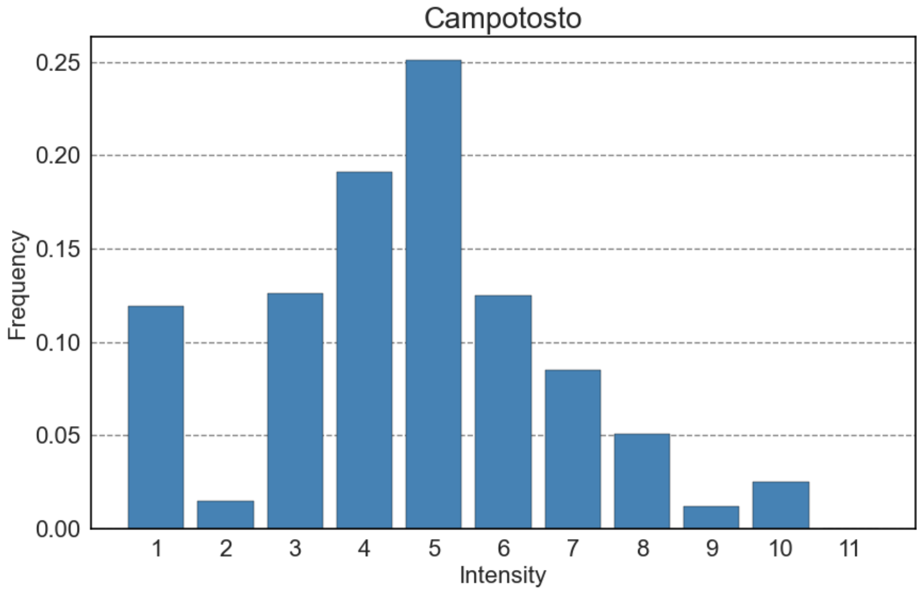

Fig. 3: Cumulative and normalised prior distribution (BNN) for MDP classes for the 27 earthquakes in Table 1 at the Campotosto site (Central Italy). In the case of MDP, with uncertainties between two contiguous MDP values (e.g. V-VI), we assigned a weight of 0.5 to each.

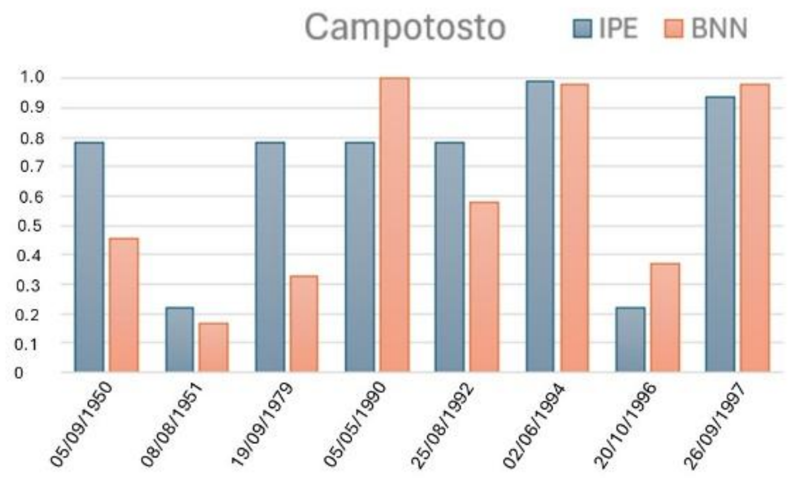

Fig. 4: histograms of probability-of-exceedance or equal to VII $P(I \geq I_{obs})$ for eight earthquakes having the same intensity value, computed by IPE (Lolli et al. 2024) and by Bayesian Natural Neighbour (taking the MDP with maximum probability as shown in Eq. 12).

As a rough example of hazard application, if we consider the period of events T=2017-1639 = 378 years, the total annual average rate is λ = n_e/T= 0.0714. One can obtain the annual rate by intensity

$$\lambda_k = \lambda \cdot \; P(I = k) \qquad (15)$$

or better for $P(I \geq k)$

$$\lambda(I \geq k) = \lambda \cdot P(I \geq k) \; (16)$$

It follows that if $P(I \geq 7) = 0.167$, then $\lambda(I \geq 7) = 0.0714 \times 0.167 \approx 0.0119$ year^{-1}, that is on average, approximately one instance that exceeds level VII every 84 years.

Table 1 also presents the comparison of the probability-of-exceedance or equal to I_{obs} [$P(I \geq I_{obs})$], computed by IPE (Lolli et al. 2024) and the present method. Using the LOGLIN formulation from Lolli et al. (2024), with the parametres from their table 1 results in a sharp distribution for both methods. The rows in light grey in Table 1 highlight eight earthquakes with the same MDP evaluated by both methods (note that Bayesian NN does not directly provide the intensity values, here we show the MDP values with maximum probability by Eq. 12). The purpose of this brief comparison is summarised in Fig. 4, which shows heterogeneity between methods, with IPE overestimating in some cases, while there is a correspondence for the highest probability.

3.2 Discrete probability maps of the MDP dataset

One problem with MDP distributions is the limited data available for many earthquakes in the catalogues. In this regard, Antonucci et al. 2021 proposed an interesting method also based on a Bayesian approach. As in our case, this method aims to integrate incomplete MDP distributions through probabilistic evaluation. However, both approaches provide probabilistic assessments rather than MDP, so there are other ways to interpret the results.

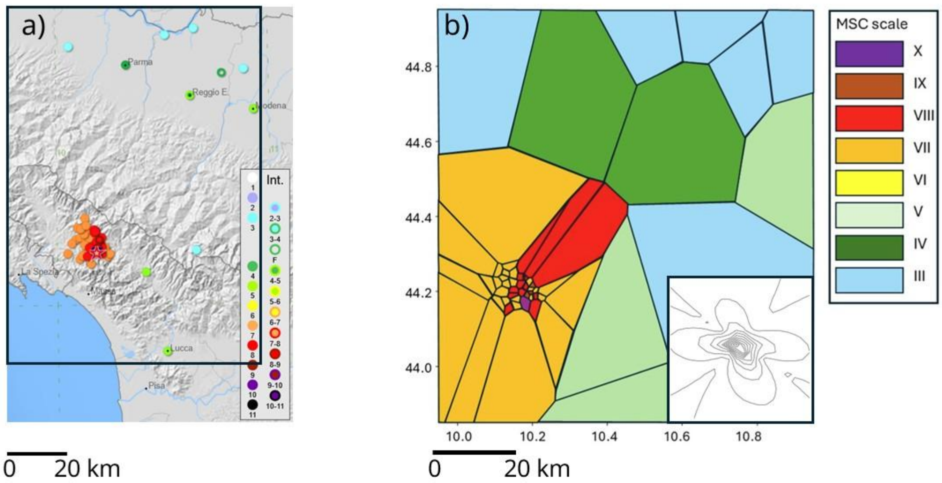

Fig. 5: a) Map of MDP for the M_w 5.8, 11 April 1837 Lunigiana (Italy) earthquake from the CPTI15 catalogue (modified from Rovida et al. 2022). The area within the black-bordered rectangle contains the MDP tessellated in figure (b). In **b)**, we omitted the data points to better represent the Voronoi polygons in the epicentral cluster. The coordinates of the epicentre are: Lat. 44.175 N; Lon. 10.182 E. The small box on the right shows the S-waves radiation pattern of the source obtained by KF inversion (Eva et al. 2025 – fault plane solution 126°, 34°, -94°). The MDP ranges from degree III to degree X, with a degree VI absent. The numbers of top degrees are 2 IX and one X (purple Voronoi in the cluster of Fig. 5b).

We apply the concept of a soft Bayesian prior probability to the M_w 5.8, 11 April 1837 Lunigiana (Italy) earthquake. Fig. 5a shows the geographic map of data from the CPTI15 catalogue (Rovida et al. 2022), used also for the macroseismic inversion to retrieve information about its source (Eva et al. 2025). The map displays a cluster of MDPs concentrated in the epicentral area (Lat. 44.175 N; Lon. 10.182 E) and scattered MDPs of lower intensity farther from the epicentre. This is more clearly visible in Fig. 5b by the Voronoi tessellation of the earthquake (we omitted the control points of the sites since they can mask the small polygons of the epicentral area). In the dataset of the 1837 earthquake, the uncertainties between two contiguous MDP values are assigned to the lowest-level values, in accordance with the decision for the inversion in the work of Eva et al. (2025). The focus of that article was on studying the source, so this decision was taken because the lowest values were considered more reliable. This computational reason is different from the aims of the present work, which is primarily concerned with data processing and representation. In any case, this available dataset is useful for other purposes. One is to reconstruct the macroseismic dataset of a past earthquake such as the 1837 event, which has a scattered and clustered distribution of sites. Using equations 8, we show in the maps (Fig. 6) the probabilities split by intensity degree for the locations $\{x_i\}_{i=1}^{1600}$ of a (40 x 40) grid with known intensity $I_i \in K = \{IV, \dots, X\}$ for the 1837 earthquake. These maps provide probabilistic zoning by damage class, which is particularly suitable for historical hazard studies. In other words, for each intensity class, Fig. 6 shows where that class receives the strongest probabilistic support: *I*=VIII is heavily concentrated in the epicentral area, which is consistent with the maximum damage occurring near the source; *I*=VII is distributed over a wider band around the epicentral cluster; *I*=IV and V emerge in more peripheral areas, where the macroseismic field decays. Thus, a spatially structured, non-uniform intensity dataset is represented, as in the case of the 1837 earthquake. This representation preserves the discrete and ordinal nature of macroseismic intensity. In terms of seismic hazard, the method can be used to construct discrete probability maps of intensity, which are more informative than simple continuous interpolation (see subsequent section).

For comparison Fig. 7 shows the maps of the probability of being intensity *I*, computed with the IPE (Lolli et al. 2024) at each location $\{x_i\}_{i=1}^{1600}$ of a (40 x 40) grid. We used the LOGLIN formulation with the parametres of their table 1 (their eq. 8) and for I_E their eq. 9). Due to the sharp distribution in Fig. 4, we chose a standard deviation $\sigma = 0.7$ instead of 0.653, to smooth the results for comparison with the maps of Fig. 6. The IPE developed by Lolli et al. (2024) provides a central intensity value at each point on the grid. Therefore, at each grid point we assigned the Bayesian prior probability (Eq. 8) corresponding to the MDP calculated by the IPE. Fig. 7 shows a local consistency map of the IPE (IPE-based probabilities), indicating the extent to which the IPE forecast is locally supported by historical data through the soft prior. Where the probability associated with the IPE intensity is high, the forecast is consistent with the observed macroseismic structure. Where it is low, the prediction is less well supported locally, which could have various explanations: the maps could indicate that the IPE is overestimating or underestimating, or that the site is in a transition zone between classes (see Discussion).

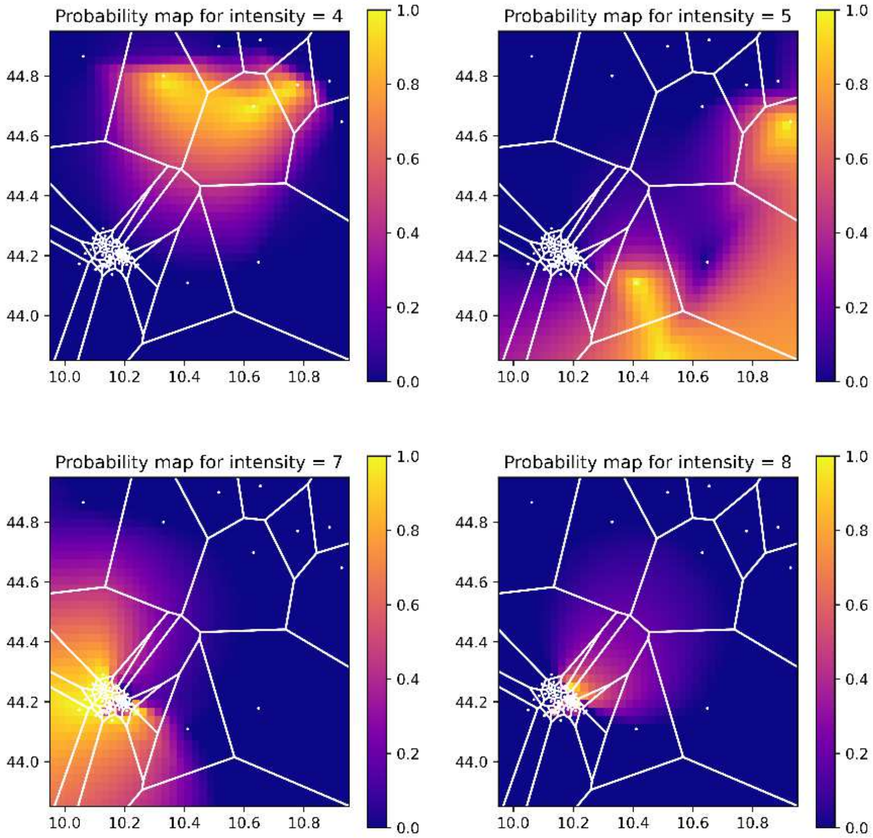

Fig. 6: Maps of BNN probabilities (Eq. 8) for MDP classes on a 40 x 40 grid for the dataset of the M_w 5.8, 11 April 1837 Lunigiana (Italy) earthquake. We show the representable MDP classes (IV, V, VII, VIII), omitting IX and X due to limited data.

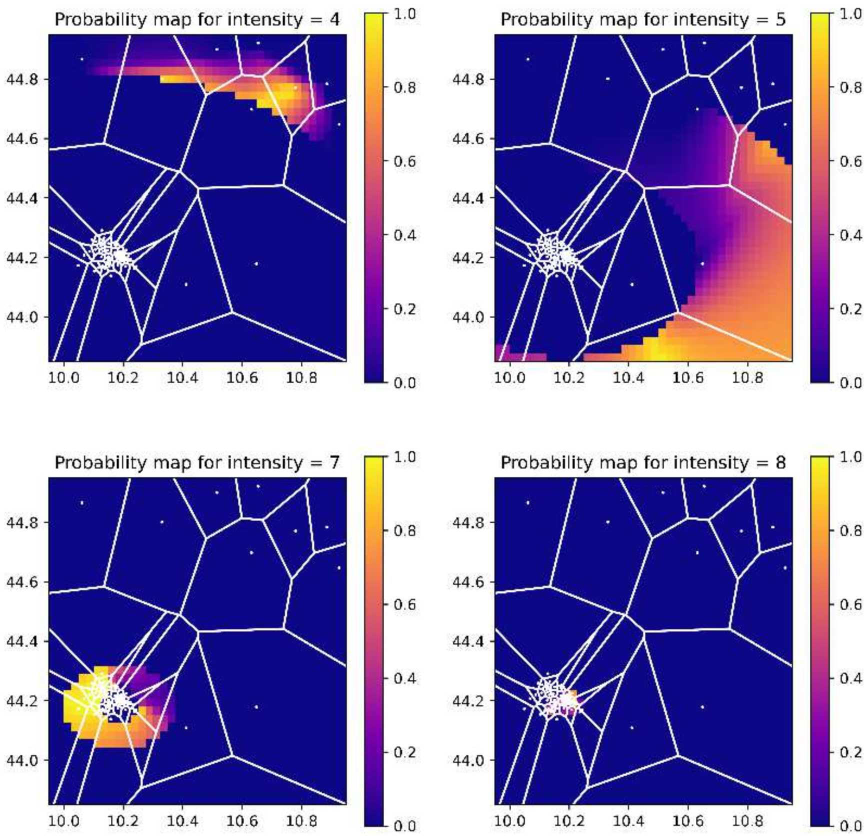

Fig. 7: Maps of the IPE-based BNN probabilities. The maps indicate the probability of having an intensity of MDP class predicted by IPE (Lolli et al. 2024).

A more informative analysis of seismic hazard involves comparing probability-of-exceedance or equal maps, $P(I \geq VII)$, calculated using the Bayesian NN method and the IPE method. The results are shown in Figures 8. Fig. 8a and 8b are maps generated using eq. (11), while Fig. 8c and 8d show the same exceedance probabilities, but computed with the IPE of Lolli et al. (2024), and as previously we used the parametres of their table 1 and $\sigma = 0.7$

$$P(I \geq J) = 1 - \Phi \frac{(J - 0.5 - \mu)}{\sigma} \qquad (17)$$

Where μ is the average value of the intensities J by IPE, and Φ is the cumulative distribution function of the standard normal distribution (Pasolini et al. 2008).

Fig. 8a, which shows the probability in the epicentral area $P(I \geq VII)$, displays a spatial structure attributable to the radiation pattern. By contrast, the map generated with the IPE (Fig. 8c) shows isotropic radiation. The detail of the site with MDP = V (see Figures 5, coord. 10.411E; 44.109N) is not secondary; the $P(I \geq VII)$ is greater than 0.6, while it is zero for BNN. The radiation pattern forms the basis of the KF inversion method, which was used to reconstruct the 1837 earthquake source (Eva et al. 2025 - see the lower panel of Fig. 5b). In simple terms, BNN displays heterogeneity, while IPE-based probabilities show a simplified but seismologically organised field. Figures 8b and 8d provide an example of the reconstruction of the 1837 MDP map, integrating 916 sites included in the area shown in Figures 5 (excluding the sites in the observed MDPs), collected from the CPTI15 catalogue.

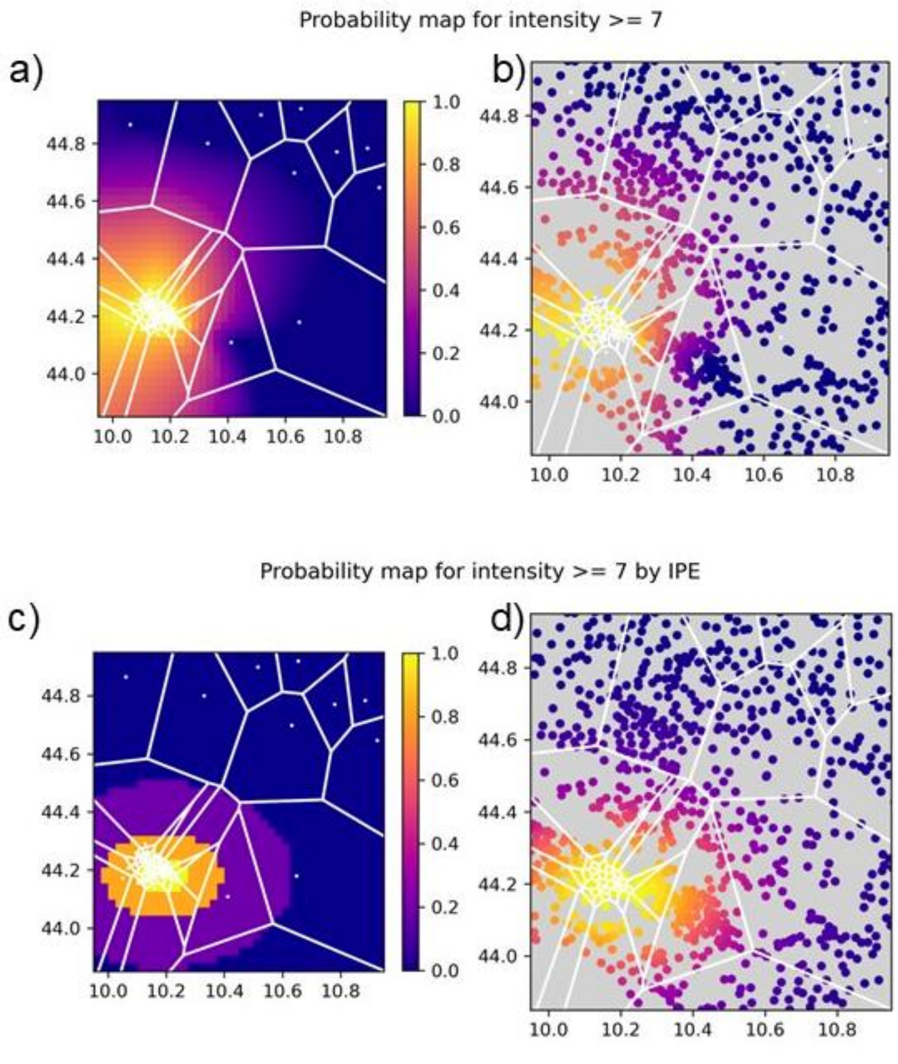

Fig. 8: Maps of exceedance $P(I \geq VII)$; **a)** probabilities computed by BNN on a 40 x 40 grid; **b)** probabilities computed by BNN on the 916 sites (excluding the sites from the 1837 dataset) to illustrate a hypothetical densification of the dataset; **c)** probabilities computed by BNN for

intensities $\geq VII$ obtained by IPE (Lolli et al. 2024); **d)** probabilities for intensities $\geq VII$ from the IPE at the 916 sites collected from the CPTI15 catalogue for the considered area of 1837 earthquake.

3.3 Discrete uncertainties for NN interpolation

In a previous article (Iurcev and Pettenati 2023), we attempted to compute the spatial uncertainty of a Natural Neighbour interpolation for all types of data. The method is based on the Lagrange theorem (Mean Value Theorem) and requires computing around the interpolation point $\boldsymbol{x}^*$, the gradient of the unknown function using least-squares strategies. One issue was the method used to select the dataset for gradient estimation: common sense suggested using natural neighbours, but the search radius proved to be the best method. The arbitrary choice of a search radius and the issue regarding the location of the Lagrange point discouraged further investigations. Additionally, a geostatistical approach was abandoned due to the arbitrary selection of a variogram (Chilès and Delfiner 1999) despite the promising results. The Bayesian NN, in the case of discrete data, provides a straightforward way to solve this problem, considering that in the 'weighted' statistic, the expected value E is simply given by the Eq. (3)

$$E[I^*] = \frac{\sum_{i=1}^{n} w_i I_i}{\sum_{i=1}^{n} w_i} \qquad (16)$$

and the variance

$$\sigma^2 = \frac{\sum_{i=1}^{n} w_i (I_i - E[I^*])^2}{\sum_{i=1}^{n} w_i} \qquad (17)$$

in view of the normalisation (4b) and the (8). Therefore, the standard deviation will be

$$\sigma = \sqrt{\sum_k P(k)(k - E[I^*])^2} \qquad (18)$$

Fig. 9a shows the isoseismals by Sibson (1981) interpolation of the M_w 5.8 11 April 1837 earthquake and in Fig. 9b there are the uncertainties in real numbers – between values of 0 and 2 - computed on the points of a grid 100 x 100 within the limits of the area.

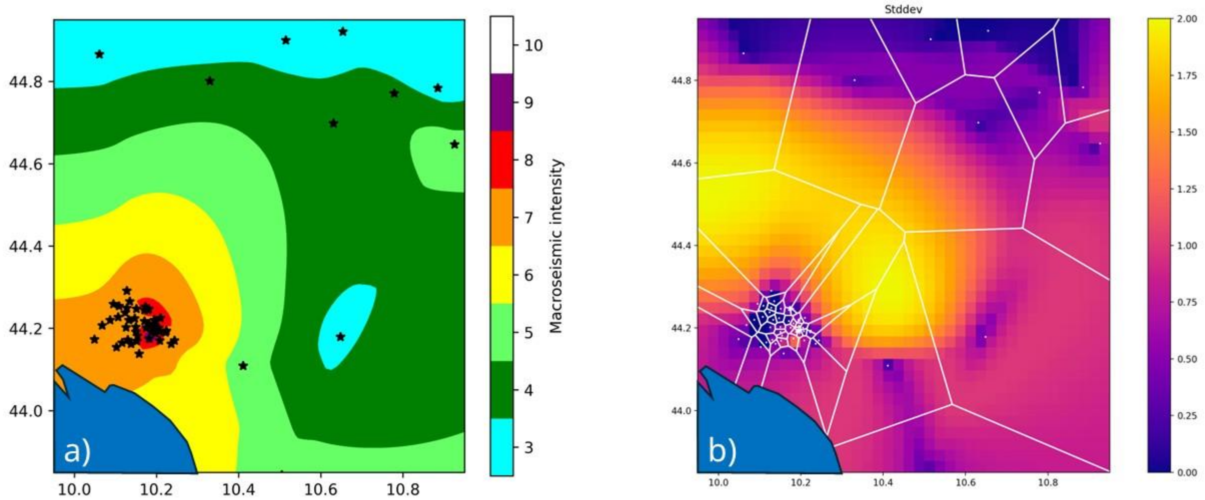

Fig. 9: a) Isoseismals for the Mw 5.8, 11 April 1837 Lunigiana (Italy) earthquake dataset from CPTI15 (Rovida et al. 2022), interpolated using the Natural Neighbour method (Sibson 1981; Iurcev and Pettenati 2023); **b)** uncertainties of isoseismals computed using equation 18.

Discussion

We refer to this reinterpretation as Bayesian Natural Neighbours. Sibson's method (1981) is traditionally geometric/deterministic, but we propose a probabilistic reinterpretation, where interpolation weights are treated as conditional probability over discrete variables. The transformation of a deterministic method into a stochastic one is generally not trivial, at least from a theoretical and idealised point of view. However, it is by no means impossible. In many scientific and technical fields, there is often a deliberate switch from deterministic to stochastic models. In Geostatistics, for example, scalar fields (e.g. permeability) are often converted into random fields (Chilès and Delfiner, 1999). A more recent example is machine learning, where Bayesian models begin with deterministic formulations that are subsequently 'probabilised' (Murphy 2012).

Considering the set of natural neighbours (NN), known as '*wreaths*', we have seen that by using the weights derived from Sibson's (1981) interpolation, treated as conditional probabilities, a discrete prior distribution can be obtained (Fig. 2a, b). We then observed how the relationships between these weights change when the control point $\boldsymbol{x}^*$, is shifted (Fig. 2c), sometimes even radically to nearby positions. In figure 2 of Iurcev and Pettenati (2023) we have already shown the sudden and complex variations of the *wreaths* at each point $\boldsymbol{x}^*$in a Voronoi partition in $\mathbb{R}^2$ of a dataset $\{x_i\}$. Supplement S1 illustrates the hierarchy of adjacency among the NN polygons involved in the calculation, extending up to order '*wreath-order'* ω = 4 (Fig. S1c). In this framework, polygon are classified according to their topological distance from the polygons containing the control point $\boldsymbol{x}^*$. Consequently, a polygon of *order* ω ≥ 2 may exist only briefly and be excluded from the calculation at a neighbouring point. In Supplement S2, for regular geometric shapes (hexagonal polygons), we observed that the shape of the polygon at point $\boldsymbol{x}^*$ (a second-order polygon – the red one in Fig. 1a) significantly affects the calculation. Therefore, when conducting a statistical test to assess the robustness of the method with respect to Sibson's interpolation values, and more specifically the weights, the error caused by randomly changing the positions is not very significant, whereas the gap resulting from the removal of a data point is significant (see Supplement S3).

For the hazard test at a single site, Campotosto has proved to be of interest, as it has been associated with 27 earthquakes, each with at least 20 data points (the key requirement is that the site has at least 2 NN around the sample site). This underlines that the method is heavily data-driven. While, this may seem obvious, it is important for applying the method. The probabilistic prior distribution (Fig. 3) also shows a probability for "not felt", which is important information. The probability $P(I \geq IX)$, is due to the major earthquake of M_w6.7 in 1703. The estimate of annual average rate means that there is an event about every 14 years (0.0714^{-1}), but perhaps it is better to consider all return period T_r = 500, so λ = n_e/T_r = 27/500 = 0.054, which means one every 18.5 years. This rough estimate is intended only to demonstrate the usefulness of the method. Table 1 reports the probability-of-exceedance or equal to VII, for each of the 27 earthquakes used for the test on Campotosto. The results shown in Fig. 4 indicate that the probability distributions derived from the IPE of Lolli et al. (2024) and from the Bayesian NN approach display consistent trends only for the earthquakes on 08/08/1951, 02/06/1994, and 26/09/1997. For the other events, the IPE probability is generally, higher. In addition, Table 1 suggests a tendency for the IPE to overestimate the observed and Bayesian NN intensities at the Campotosto site.

Moving on to the analysis of the M_w5.9, 11 April 1837 earthquake, the initial idea of integrating the dataset with MDP from other sites not observed in its CPTI15 catalogue is less interesting than comparing Fig. 6 with Fig. 7 for hazard purposes. This comparison is valuable from an interpretative perspective, as the figures illustrate two different but complementary aspects: Fig. 6 indicates where a certain class of intensity is most supported by the geometry and the historical observed data, while Fig. 7 shows where the MDP predicted by the IPE is locally consistent with the local macroseismic probability of historical data. The map in Fig. 6 does not yet represent seismic hazard in the conventional sense, but it provides a spatial probabilistic representation of the occurrence of each intensity class. The first set of maps (Fig. 6) identifies the areas where each class of macroseismic intensity is most strongly supported locally by the ‘Natural Neighbours’ Bayesian prior. The second set of maps shows, for each grid point, the probability associated with the MDP predicted by the IPE. Taken together, these results suggest that the proposed method can provide a site-dependent measure of consistency between empirical macroseismic evidence and model-based intensity prediction, which could prove useful in intensity-based seismic hazard applications. In terms of hazard: Fig. 7 does not necessarily alter the attenuation model, but it does modulate its local credibility. For example, in Fig. 7, the probabilities in the southeastern part of the map strongly support I = V, while the MPD = III (Fiumalbo), represented by the large polygon, in the eastern part (see also Fig. 5b), is debatable. The map in Fig. 7 thus transforms a theoretical forecast into a locally weighted forecast. In any case, for $P(I \geq VII)$ and $P(I = IV)$ low probability values in Fig. 6 follow the outline of the polygons, extending into the areas of adjacent polygons, including the central region where the missing grade VI MDPs are expected to be found. This highlights a limitation of BNN methods that is dependent on the data. Indeed, also Fig. 9b clearly shows the absence of VI MDPs in the dataset; the maximum errors occur in the central (yellow) zone, which marks the transition between the epicentral area and the outer low-intensity zone. This finding, resulting from the method's objectivity, can help highlight the dataset's shortcomings.

Figures 8a–b (Bayesian Natural Neighbours) and 8c–d (IPE-based probabilities) display markedly different spatial patterns. The BNN approach generates a highly heterogeneous probability field, strongly influenced by the spatial distribution of observations and able to capture local variability, which is inherently lost in the model-based IPE representation. By contrast, the IPE-based maps (Figures 8c-d) present smoother and more regular patterns, primarily determined by the distance from the epicentre and the assumed attenuation model. This suggests that the two approaches are complementary, with the BNN framework proving a data-driven refinement of hazard patterns derived from empirical attenuation models. The heterogeneity shown by the BNN can be useful for analysing the radiation pattern of the earthquake, as in the case of Fig. 5c and as we considered in Pettenati et al. (1999 – figure 3), when comparing the radiation pattern of the source solution of an earthquake, with the model derived from IPE. Finally, the integration of IPE and soft prior data enables distinction between expected intensities that are well supported locally and those that are only weakly supported.

The selection of the 11 April 1837 M_w5.9 earthquake dataset is deliberate; the absence of VI-grade MDPs, as also seen in Fig. 2b, underscores the inherent limitation of the method, which depends solely on the spatial relationships within the data and intrinsic conditional probability. However, this method does not employ search circles, which attract subjective criticism; it maintains the discrete and ordinal nature of macroseismic intensity; avoids imposing artificial continuity between classes (as in interpolation); and instead generates probabilistic zoning by damage class, making it highly suitable for historical hazard studies. This could prove very important as it leads to hazard models that incorporate historical information, local spatial structure, and consistency with observed data. Using prior distributions makes operations on these discrete and ordinal variables more mathematically sound. The method also offers a potentially more accurate way of representing the data than contours and interpolations. Figure 10 shows the distribution of MDPs, using Eq. (12) to create discrete maps - the Maximum a Posteriori (MAP). The versatility of the BNN method also enables other applications, such as: 1) studying a new method to integrate the probability of the missing MDP classes into the soft prior distributions; 2) studying local effects in historical earthquake MDP maps; 3) using weights in inversion methods, where, in each site, for every iteration, the calculated MDPs are weighted with the corresponding probability derived from the soft prior; 4) possible extension on real variables as a map in frequency of HVSR measurement of a deep basin (Laurenzano et al. 2023).

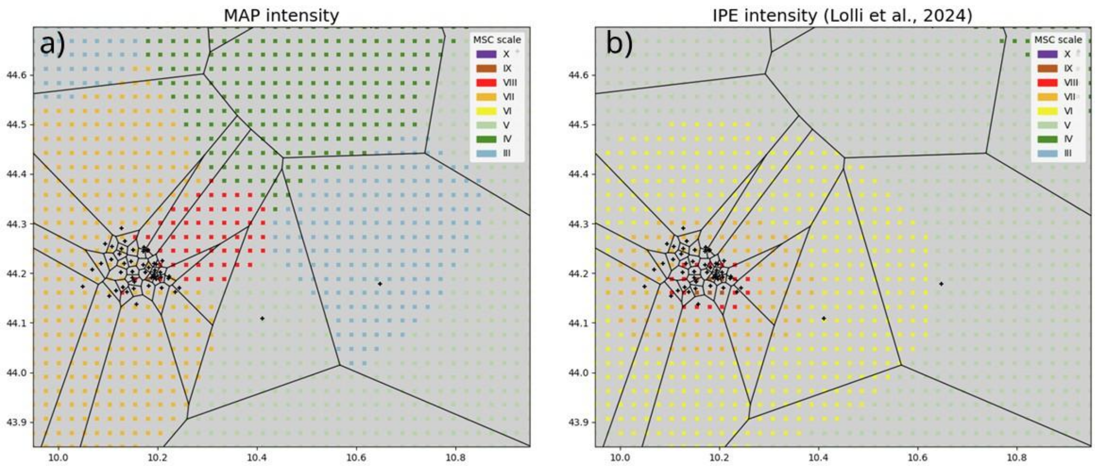

Fig. 10: a) Map of the discrete distribution of MDPs, calculated by BNN using equation (12) on a 40 x 40 grid; **b)** map of the discrete distribution of MDPs computed with the IPE of Lolli et al. (2024), on a 40 x 40 grid.

Conclusion

In this study, we applied the Bayesian Natural Neighbours (BNN) method to derive soft prior probability distributions of macroseismic intensity directly from observed data. At each location, the approach provides a discrete probabilistic description of intensity, obtained as a weighted combination of neighbouring observations through the Sibson (1981) formulation. The method is simple, but it is entirely objective, depending solely on the spatial relationships within the data and intrinsic conditional probability which is contained in the Sibson method.

The robustness of the method was assessed by analysing the sensitivity of soft prior distributions to variations in the spatial configuration of the data. The results show that the method performs well under typical conditions, although it becomes less stable when one or more nearest neighbours are removed, highlighting its dependence on the local geometry of the data.

The application to the 11 April 1837 M_w5.9 Lunigiana earthquake demonstrates the relevance of the BNN framework for seismic hazard analysis. The resulting probability maps capture significant spatial variability and reproduce local features not described by traditional Intensity Prediction Equations (IPEs). The flexibility of the BNN framework enables its integration with IPE-based approaches, as shown in Fig. 7, where soft prior distributions are combined with probabilistic estimates from attenuation models. It should be noted that the application to the 1837 dataset is affected by the absence of certain intensity classes (e.g. degree VI), which may limit the completeness of the inferred distributions. Ongoing work aims to address this limitation by developing strategies to handle missing intensity classes and further improve the integration between BNN and IPE approaches. These results show that the BNN approach can implicitly incorporate source-related anisotropy directly from the data, providing a data-driven complement to model-based methods and offering improved insight into the spatial variability of seismic intensity for hazard assessment.

Funding

No funding was obtained for this study.

Data availability

This study did not generate new observational datasets. The earthquake parameters and macroseismic data used in the analyses were obtained from the CPTI15 catalogue (Rovida et al., 2022).

References

Antonucci, A., A., Rovida, V., D'Amico, and D., Albarello (2021). Integrating macroseismic intensity distributions with a probabilistic approach: an application in Italy. *Nat. Hazards Earth Syst. Sci.*, 21, 2299–2311, 2021 https://doi.org/10.5194/nhess-21-2299-2021

Aurenhammer, F., Klein, R., Lee, D. (2013). *Voronoi Diagrams and Delaunay Triangulation*. World Scientific Publishing Co. Pte. Ltd., 348. https://doi.org/10.1142/8685.

Bakun, W. H., and Wentworth, C. M. (1997). Estimating earthquake location and magnitude from seismic intensity data, *B. Seismol. Soc. Am.*, 87, 1502–1521.

Backus, G.E. (1988). Comparing hard and soft prior bounds in geophysical inverse problems. *Geoph. J. Int.*, vol. 94, Issue 2, August 1988, Pages 249–261, https://doi.org/10.1111/j.1365-246X.1988.tb05899.x

Barnes, S.L. (1964). *A technique for maximizing details in numerical weather-map analysis*. *J. Appl. Meteorol. Climatol.*, 3, 396-409, doi: 10.1175/1520-0450(1964)0030396:ATFMDI>2.0.CO;2.

Burrough, P. A., and R. A., McDonnel (1998). Principles of Geographic Information Systems. OUP Oxford, ISBN-13: 978-0198233657, 352 pp.

Chilès, J. P., and Delfiner, P.; (1999). *Geostatistics*. *Modeling Spatial Uncertainty.* Wiley Series is Probability and Statistics, 695 pp.

Eva, E., Molli, G., Pettenati, F., Solarino, S. (2025). Seismicity, seismotectonics and historical earthquakes of the Northwestern Apennines, Italy: A reappraisal. *Tectonophysics* 898 (2025), https://doi.org/10.1016/j.tecto.2025.230642.

Friston, K.J., Penny, W., Phillips, C., Kiebel, S., Hinton, G., and Ashburner, J. (2002). Classical and Bayesian inference in neuroimaging: Theory. *NeuroImage*, 16(2), 465–483. https://doi.org/10.1006/nimg.2002.1090

Gandin, L.S. (1965). *Objective analysis of meteorological fields*. U.S. Department Commerce and National Science Foundation, Washington, D.C., USA, 242 pp.

Gentile, F., F., Pettenati, and L., Sirovich, (2004). Validation of the Automatic Nonlinear Source Inversion of the U. S. Geological Survey Intensities of the Whittier Narrows, 1987 Earthquake. *Bull. Seism. Soc. Am.*, vol.**94**, No.5, 1737-1747, October 2004, https://doi.org/10.1785/012003157.

Gasperini, P, Bernardini, F, Valensise, G., and Boschi, E. (1999). Defining seismogenic sources from historical earthquake felt reports, B. *Seismol. Soc. Am.*, 89, 94–110.

Goovaerts, P. (1997). *Geostatistics for natural resources evaluation*. Oxford Uni, New York.

Iurcev, M., and F., Pettenati (2023). Exploring error estimation methods for natural neighbour interpolation: preliminary research and analysis. Bull. Geoph. Ocean. Vol. 64, 4, 433-448, December 2023. https://doi.org/10.4430/bgo00423.

Laurenzano, G., M., Garbin, S., Parolai, C., Barnaba, M., Romanelli, and L., Froner (2023), High-resolution local seismic zonation by cluster and correlation analysis, *Soil Dynamics and Earthquake Engineering*, 173, 108122, doi: 10.1016/j.soildyn.2023.108122.

Lolli, B., P., Gasperini, and G., Vannucci (2024). Recalibration of the Intensity Prediction Equation in Italy Using the Macroseismic Dataset DBMI15 Version 2.0, *Seismol. Res. Lett.* 95, 2399–2408, doi: 10.1785/0220230212.

Kövesligethy, R. (1907). Seismischer Stärkegrad und Intensität der Beben, Gerl. Beitr. Geophys., Bd. 8, 24–103.

Mallet, R. (1862). *The Great Neapolitan Earthquake of 1857*, 2 vols., Chapman and Hall, London, 431, 399 pp.

Mercalli, G. (1902). Sulle modificazioni proposte alla scala sismica De Rossi–Forel. Boll. Soc. Sismol. Ital. 1902, 8, 184–191. (In Italian).

Moratto, L., Santulin, M., Tamaro, A., Saraò, A., Vuan, A., A., Rebez (2023). Near-source ground motion estimation for assessing the seismic hazard of critical facilities in central Italy. *Bull. Earthq. Eng*. (2023) 21:53–75, https://doi.org/10.1007/s10518-022-01555-0

Murphy, K. P. (2012). *Machine Learning: A Probabilistic Perspective*. MIT Press, 1098 pp.

Okabe, A.B., Boots B., Sugihara, K., and Chiu, S.N. (2000). *Spatial Tessellation*. Second ed., Wiley, Chichester, 671 pp.

Pasolini, C., Albarello, D., Gasperini, P., D'Amico, V., and Lolli, B. (2008). The attenuation of seismic intensity in Italy, Part II: Modeling and validation, *B. Seismol. Soc. Am.*, 98, 692–708, https://doi.org/10.1785/0120070021.

Pettenati, F., L., Sirovich, and F., Cavallini (1999). Objective treatment, and synthesis of macroseismic intensity data sets using tessellation, *Bull. Seism. Soc. Am.* **89,** 1203–1213.

Pettenati, F., Sirovich, L., and Sandron, D. (2011). Rapid simulation of seismic intensitiy for civil protection purpose; two recent cases in Italy. *Seismol. Res. Lett.*, **82**, 3, 420 -430, https://doi.org/10.1785/gssrl.82.3.420.

Provost, L., and Scotti, O. (2020). QUake-MD: Open-Source Code to Quantify Uncertainties in Magnitude–Depth Estimates of Earthquakes from Macroseismic Intensities, *Seismol. Res. Lett.*, 91, 2520–2530, https://doi.org/10.1785/0220200064.

Rovida, A., Locati, M., Camassi, R., Lolli, B., Gasperini, P., Antonucci A. (2022). Catalogo Parametrico dei Terremoti Italiani (CPTI15), versione 4.0 [Data set]. Istituto Nazionale di Geofisica e Vulcanologia (INGV). https://doi.org/10.13127/cpti/cpti15.4.

Sibson, R. (1980). A vector identity for the Dirichlet tessellation. *Math. Proc. Camb. Phil. Soc.*, 87, 151-155.

Sibson, R. (1981). A brief description of natural neighbor interpolation. Interpreting Multivariate Data, V. Barnett editor, Chichester, John Wiley, 21-36.

Sirovich, L., F., Pettenati, F., Cavallini, and M., Bobbio (2002). Natural neighbor isoseismals, Bull. *Seismol. Soc. Am.* 92, 1933–1940.

Sirovich, L,. and F., Pettenati (2004). Source Inversion of Intensity patterns of Earthquakes; a Destructive Shock in 1936 in northeast Italy. *Journal of Geophysical Research*, vol. **109**, B10309, 2004, 1-16, https://doi.org/10.1029/2003JB002919.

Sirovich, L., and F., Pettenati (2009). Validation of a Kinematic and Parametric Approach to Calculating Intensity Scenarios. *Soil Dynamics and Earthquake Engineering*, https://doi.org/10.1016/j.soildyn.2008.12.007, **29**, 7, 1113-1122, July 2009.

Sirovich, L., Pettenati, F., and Cavallini, F. (2013). Intensity-Based Source Inversion of the Destructive Earthquake of 1694 in the Southern Apennines, Italy. *Journal of Geophysical Research*, vol. **118**, 1-17, 2013, https://doi.org/10.1002/2013JB010245.

Worden, B., Thompson, E.M., Baker, J.W., Bradley, B.A., N., Luco, and Wald, D.J. (2018). Spatial and Spectral Interpolation of Ground-Motion Intensity Measure Observations. *Seismol. Soc. Am.* 108(2), 866–875, doi: 10.1785/0120170201.

Table 1: Dataset of 27 earthquakes selected from the CPTI15 catalogue (Rovida et al. 2022), for the computation of the cumulative distribution of Campotosto (Central Italy) site.

Earthquake	M_w	Distance (km)	Obs. MDP (I_{obs})	MDP from IPE (+)	IPE $P(I \geq I_{obs})$	BNN (+), [*] $P(I \geq I_{obs})$
07/10/1639	6,21	12,67464	8	8	0.5	0.373 [7.5]
02/02/1703	6,67	15,18213	8	8,5	0.781	0.666 [10]
02/08/1893	4,55	30,81318	3	3,5	0.781	0.689 [5,5]
13/01/1915	7,11	61,92607	7	7,5	0.781	0.035 [7]
05/09/1950	5,7	7,369401	7,5	8	0.781	0.454 [8]
08/08/1951	5,27	12,74151	6,5	6	0.219	0.164 [6]
24/06/1958	5,02	28,83447	3	4,5	0.991	0.997 [4]
14/03/1960	4,72	58,53403	1	3	0.999	0.1 [1]
16/03/1960	4,44	7,242714	3	5	0.999	0,567 [4]
19/09/1979	5,9	25,54128	6	6,5	0.781	0.372 [6.5]
13/10/1986	4,5	42,60917	3	3	0.5	0,709 [4]
03/07/1987	5,28	86,52508	1	3,5	0.999	0.352 [3]
05/05/1990	5,77	281,6297	1	1	0.781	1 [1]
25/08/1992	4,22	5,855674	4,5	5	0.781	0.581 [5]
05/01/1994	3,87	11,54	2,5	3,5	0.939	0.977 [3]
02/06/1994	4,16	13,89933	2,5	4	0.991	0.981 [4]
20/10/1996	4,36	21,41527	4,5	4	0.219	0,368 [4]
26/09/1997	5,48	61,82528	4	4,5	0.781	0.672 [5]
26/09/1997	5,89	65,30237	4	5	0.939	0.981 [5]
05/04/1998	4,78	85,98361	3	2,5	0.219	0,007 [3.5]
10/10/1999	4,14	17,66571	2,5	3,5	0.939	0.614 [4]
09/12/2004	4,19	45,14444	1	2,5	0.991	0.552 [1]
15/12/2005	4,34	55,66306	1	2,5	0.991	0,002 [1]
06/04/2009	6,19	30,03295	6	6,5	0.781	0 [5.5]
24/08/2016	6,46	15,79921	5	8	0.999	0.112 [5]
30/10/2016	6,61	37,08818	7	7	0.5	0.828 [6.5]
18/01/2017	5,7	7,7104	8	7.5	0.219	0 [7]

(+) In the case of MDP I, with uncertainties between two contiguous MDP values (e.g. V-VI), we follow the same pattern of section 3.1 (see Fig. 3).

[*] Bayesian NN Method gives the probability values: in the square brackets the MDP values referred to the maximum BNN probability (equation 12) is reported.

Table 2: List of cumulative BNN probabilities related to each MDP for the Campotosto (Central Italy) site (Fig. 3).

MDP	Probability
1	0.119
2	0.015
3	0,125
4	0.191
5	0.251

6	0.125
7	0.085
8	0.051
9	0.012
10	0.024
11	0

Acknowledgements

We thank Lucio Torelli (University of Trieste) for insightful discussions and encouragement regarding this work, Federico Sau (Politecnico di Milano) for discussions on the analytical aspects of probability theory, and Dario Albarello (University of Siena) for helpful suggestions concerning hazard applications.

Author contributions

F.P. and M.I. contributed equally to the development of the methodology, equations, numerical tests, and figures presented in this work. F.P. conceived the Bayesian-inspired reinterpretation of the Sibson method and the use of soft prior distributions, and wrote the manuscript. M.I. contributed to the theoretical framework that inspired part of the study and participated in the development and discussion of the proposed approach.

Declarations

Competing interests

The authors declare that they have no financial or non-financial competing interests.

Additional information

Supplementary Information

Supplementary Files

This is a list of supplementary files associated with this preprint. Click to download.

- Table2.docx
- TableS1.docx
- Table1.docx
- Supplementaryv1.4.docx